Gas-Substrate Heat Exchange During Cold-Gas Dynamic Spraying

A.G. McDonald, A.N. Ryabinin, E. Irissou, and J.-G. Legoux

(Submitted June 19, 2012; in revised form September 14, 2012)

In this study, the temperature distribution of the surfaces of several substrates under an impinging gas jet from a cold spray nozzle was determined. A low-pressure cold-gas dynamic spraying unit was used to generate a jet of hot compressed nitrogen that impinged upon flat substrates. Computer codes based on a finite differences method were used to solve a simplified 2D temperature distribution equation for the substrate to produce nondimensional relationships between the surface temperature and the radius of the impinging fluid jet, the axial velocity of the cold spray nozzle, the substrate thickness, and the heating time. It was found that a single profile of the transient nondimensional maximum surface temperature could be used to estimate the dimensional maximum surface temperature, regardless of the value of the compressed gas temperature. It was found further that, as the thermal conductance of the substrate increased, the maximum surface temperature of the substrate beneath the gas jet decreased. Heat exchange between the substrate and the compressed gas jet during motion of the nozzle to produce heat conduction within the substrate was characterized by the nondimensional Peclét number. It was found that lower Peclét numbers produced higher temperatures within the substrate. The close agreement of the numerical results with the experimental results suggests that the nondimensionalized results may be applied to a wide range of conditions and materials.

1. Introduction

Cold spraying is a coatings fabrication process in which small, un-melted metal or alloy powder particles (1-100 μm in diameter) are accelerated to high speeds (500-1200 m/s) by a supersonic gas jet to form a dense protective or functional coating (Ref 1-4). The high speed of the particles at impact promotes plastic deformation to form strong bonds within the coating (Ref 5-8). While it has been shown extensively that spray parameters such as the gas

temperature and pressure affect the adhesion of the particles during deposition to fabricate the coating (Ref 1-3, 9), substrate preheating has also begun to receive wide attention in the development of high-quality cold-sprayed coatings.

Previous studies have shown that the substrate surface temperature will affect the deposition behavior of cold-sprayed metals and the final fabrication of the coatings. Fukumoto et al. (Ref 10), through fundamental analysis of individual particles, have shown that increasing the temperature of mirror-polished stainless steel and aluminum substrates will increase the deposition rate of cold-sprayed copper particles. Wong et al. (Ref 11) also found that an increase in substrate surface temperature produced higher deposition efficiencies.

Study by Legoux et al. (Ref 12), which focused on the effects of surface temperature variation on the microstructure of macroscopic aluminum and tin coatings, showed that increasing the substrate surface temperature increased the particle deformation within the coating and the coating-substrate contact. This has led other investigators (Ref 13) to show that, as the substrate temperature increases, the adhesion strength of the coating to the substrate increases.

Surface heating has been combined with cold spray deposition to improve the overall quality of the final coatings. Kulmala and Vuoristo (Ref 14), Danlos et al. (Ref 15), and Lupoi et al. (Ref 16) have combined cold spraying with laser-assisted surface heating to improve the deposition efficiency, density, and adhesion strength of copper-alumina, nickel-alumina, and aluminum coatings onto either steel or aluminum 2017 alloy substrates. The study of Rech et al. (Ref 17) has indicated that a limited

AG. McDonald, Department of Mechanical Engineering, University of Alberta, 4-9 Mechanical Engineering Building, Edmonton, AB T6G 2G8, Canada; **AN. Ryabinin**, Institute of Mathematics and Mechanics, St. Petersburg University, St. Petersburg, Russia; and **E. Irissou** and **J.-G. Legoux**, National Research Council Canada, Boucherville, QC J4B 6Y4, Canada. Contact e-mail: andre.mcdonald@ualberta.ca.

increase in the residual stresses in pure aluminum coatings deposited on pre-heated 6061 aluminum occurred. The substrate surface was heated by electrical heaters.

Modification of the substrate surface temperature has produced improvements in the overall microstructural quality of the final coatings. However, management of heat transfer to temperature-sensitive substrate materials will be required. Numerical modeling has proved to be an efficient method to study the influence of the substrate surface temperature on the deposition and fabrication of cold-sprayed coatings. Studies by King et al. (Ref 5, 18) have shown that the effect of substrate heating by the hot compressed gas jet cannot be ignored during modeling of the impact of individual particles in cold spraying. More recently, other investigators (Ref 19-21) have begun to conduct heat-transfer analysis of the substrate temperature distribution and study the interaction of the gas jet with the substrate. In particular, Li et al. (Ref 20) used a commercial FLUENT code to model the temperature distribution in the substrate under a stationary jet from a cold spray nozzle. However, motion of the jet in cold spraying is more typical. Therefore, with the exception of the above cited few studies, widespread analyses of the fundamental heat transfer between the cold spray compressed gas jet and the substrate surface still needs to be explored.

The present study examines the surface temperature of the substrate during impingement by the compressed gas jet of a cold spraying nozzle. means of experimentation and numerical simulation, the relationship between the surface temperature and the radius of the impinging fluid jet, the axial velocity of the cold spray nozzle, the substrate thickness, or the heating time is determined.

2. Experimental and Numerical Methods

A low-pressure cold-gas dynamic spraying system (SST Series P, Centerline, Ltd., Windsor, ON, Canada) was used to generate a jet of hot compressed nitrogen. The pressure and the temperature range of the nitrogen gas were 690 kPa (100 psig) and 100-400 °C, respectively, as measured at the cold spray system console. The converging-diverging de Laval nozzle in the cold spray torch was 140 mm long, had a throat diameter of 2.54 mm, and an exit diameter of 6.3 mm. During operation, the cold spray nozzle was manipulated by a robot (Motoman-HP20, Yaskawa Electric Corporation, Waukegan, IL, USA). The stand-off distance (SOD), the distance between the nozzle and the substrate, was fixed at 10 mm for most tests. For stationary nozzle tests, the nozzle was moved to the center of the substrate at a speed of 1 m/s and held there. For moving nozzle tests, the nozzle was moved to scan a line through the center of the substrate at traverse speeds ranging from 2 to 150 mm/s.

The substrates were mounted on a substrate holder, and a thermo-insulator material (Alumina Insulation Type SALI Al_2O_3-SiO_2, ZIRCAR, Florida, NY, USA) was placed between the substrate and the holder. Figure 1 shows a schematic of the assembly. The insulation was used to restrict the heat exchange between the ambient air and the substrate surface only. A blower was used to create airflow of approximately 3.8 m³/s (8050 cfm), ensuring a constant ambient room temperature for heat exchange in proximity to the substrate. A variety of substrate materials, prepared in square geometries, were considered. Copper, pure aluminum, aluminum 6061 alloy, steel 1020, stainless steel 304, brass, and Lexan (SABIC Innovative Plastics, Pittsfield, MA, USA) were used. Lexan is a polycarbonate resin thermoplastic with low thermal conductivity (0.2 W/m K). The substrates had a square dimension of 76.2 mm and the thickness varied from 0.5 to 6.2 mm. Table 1 shows the thermal properties of the substrates that were used in this study.

Steady-state temperature measurements of the surface of the substrates were taken by means of an infrared camera (ThermaCAM SC-Series 3000, FLIR Systems, Sweden). The camera had a spatial resolution of 1.1 mrad, a spectral range of 8-9 μm, and a time resolution of 17 ms. The 17 ms was calculated from a frame rate of 60 Hz. The frame frequency was 60 frames per second. In order to approach ideal black-body radiation, the substrate surface was painted black with a high-temperature paint that had an emissivity of 0.95.

Computer codes based on a finite differences method were generated to solve the governing temperature distribution equations and determine the substrate surface temperature beneath the impinging, spreading jet. A
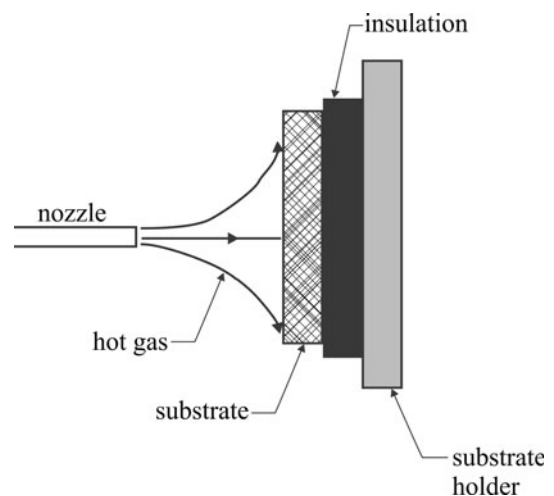

Fig. 1 Schematic of the substrate assembly

Table 1 Thermal properties of the substrates

Material	Thermal conductivity, k_s, W/m K	Density, ρ_s, kg/m³	Specific heat capacity, c_{ps}, J/kg K
Lexan	0.2	1200	1210
Stainless Steel 304	25	7800	460
Steel 1020	52	7870	486
Pure aluminum	210	2699	900
Aluminum 6061	180	2700	896
Copper	385	8960	385
Brass	115	847	380

Runge-Kutta fourth-order method was employed by the time solver. The codes were written in Pascal, and the maximum number of grid points was 11,000. For the case of the moving cold spray nozzle, the dimensionless time step parameter, $(V\Delta t/\Delta x)$, was less than 1 for calculations of the temperature distribution.

3. Description of Mathematical Model

The impingement of a hot supersonic gas jet onto a solid surface will result in rapid surface heating near the impingement or stagnation point of the jet. Estimation of the heat transfer coefficient (h) of the spreading gas film, which is directly proportional to the heat transfer rate from the gas to the solid surface, will need to be conducted. Ryabinin et al. (Ref 21) have developed a simple heat transfer model to estimate the radial heat transfer coefficient under a compressed nitrogen jet in the cold spraying process. The model developed by Ryabinin et al. (Ref 21) can be used directly, after determination of the heat transfer coefficient, to estimate the substrate surface temperature. An abbreviated summary of the model is presented here. Figure 2 shows a schematic of the model. The supersonic jet impacts upon the surface to spread axisymmetrically as a thin gas film on the solid surface at $z = l$ (see Fig. 2). All the other sides of the solid substrate were modeled as being insulated. The thickness of the substrate ($0 < z < l$) was much smaller than the length ($0 < x < L$) and height ($0 < y < H$). For substrates with small thickness and/or high thermal conductivities, the temperature variation through the cross section of the thickness will be small. Therefore, the governing 3D heat conduction equation was reduced to a 2D form to give an approximate substrate temperature distribution (Ref 21):

$$\frac{1}{\rho_s c_{ps} l}\left[k_s l\left(\frac{\partial^2 T}{\partial x^2} + \frac{\partial^2 T}{\partial y^2}\right) + h[T_{aw} - T(x,y,l,t)]\right] = \frac{\partial T}{\partial t},$$
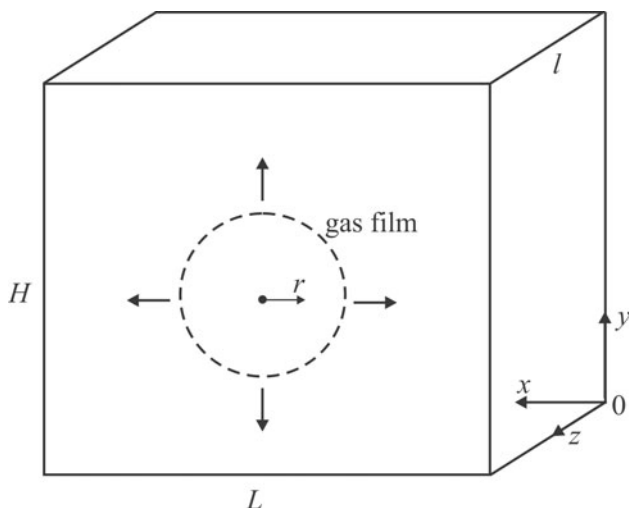(Eq 1)

Fig. 2 Schematic of the jet on the substrate surface (Ref 21)

where h is the heat transfer coefficient, and T_{aw} is the adiabatic wall temperature.

The boundary conditions and initial condition are

$$\frac{\partial T(0,y,t)}{\partial x} = 0,$$
(Eq 2)

$$\frac{\partial T(L,y,t)}{\partial x} = 0,$$
(Eq 3)

$$\frac{\partial T(x,0,t)}{\partial y} = 0,$$
(Eq 4)

$$\frac{\partial T(x,H,t)}{\partial y} = 0,$$
(Eq 5)

$$T(x,y,0) = T_i.$$
(Eq 6)

4. Results and Discussion

4.1 Substrate Surface Temperature Distribution

The computational determination of the adiabatic wall temperature (T_{aw}) shown in Eq 1 is associated with the involvement of complex mathematical models and requires significant computational resources. To alleviate these difficulties, the infrared camera was used to measure the radial surface temperatures of Lexan (low thermal conductivity material) and steel 1020 plates under the gas film (see Fig. 3). These temperatures were measured after steady-state and equilibrium was established. Owing to its low thermal conductivity, the Lexan surface temperatures represented approximate values of the adiabatic wall temperatures under the spreading, compressed hot gas film. Figure 3 shows the temperature variation of the surface of Lexan and steel 1020 under the impinging gas jet. The gas temperature and pressure, as measured at the console of the cold spray unit, was 100 °C and 621 kPa (90 psig), respectively. The SOD was 10 mm. As expected, the surface temperature close to the stagnation point ($r = 0.0$ mm) of the hot jet was higher on Lexan because of its lower thermal conductivity. With known values of the adiabatic wall temperature, Eq 1 was applied to estimate and verify the spatially varying heat transfer coefficient (h) of the spreading gas jet. Values of the heat transfer coefficient are presented elsewhere (Ref 21).

As shown in Fig. 3, the maximum surface temperature of the substrates occurs beneath the central stagnation point of the compressed gas jet. Figure 4 shows that, for steel 1020, as the temperature of the compressed gas jet (measured at the cold spray unit console) increases, the maximum surface temperature increases. The figure also shows that thermal equilibrium (steady state) is attained after approximately 40 s. A representation of the temperature variation in nondimensional form will expand the applicability of the results presented in this study. To this end, the dimensional transient maximum surface temperature profiles presented in Fig. 4(a) are presented in nondimensional form in
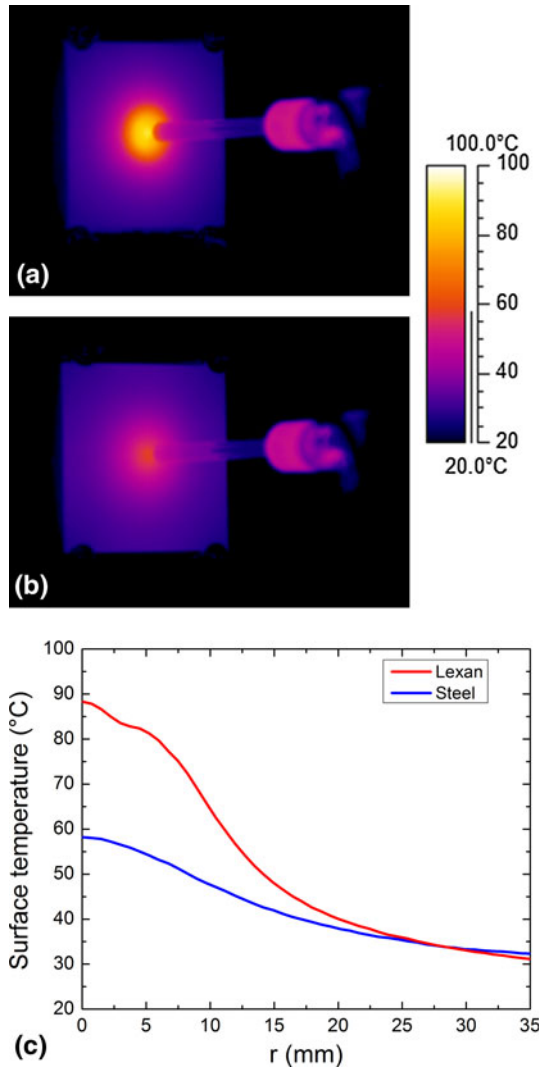
Fig. 3 Thermal image of (a) Lexan, (b) steel 1020, and (c) surface temperature profiles on Lexan and steel 1020

Fig. 4 (a) Dimensional and (b) nondimensional transient maximum surface temperature of steel 1020 under gas jet

Fig. 4(b). Only the temperature was nondimensionalized as

$$\theta = \frac{T_w - T_\infty}{T_g - T_\infty}. \qquad \text{(Eq 7)}$$

T_g is the temperature of the compressed gas jet, T_w is the measured substrate surface temperature, and T_∞ is the ambient temperature, which was equal to 21 °C. The use of a nondimensionalized temperature parameter (θ) produced profiles that coalesced (see Fig. 4b). This suggests that the nondimensional temperature curve can be used to estimate the substrate surface temperature at the stagnation point of the compressed gas jet for any gas temperature, other than those presented in Fig. 4. The profiles coalesced because of the proportional relationship between the gas temperature and the surface temperature at the stagnation point. Further, given that the back of the substrate was insulated, no convection occurred there,
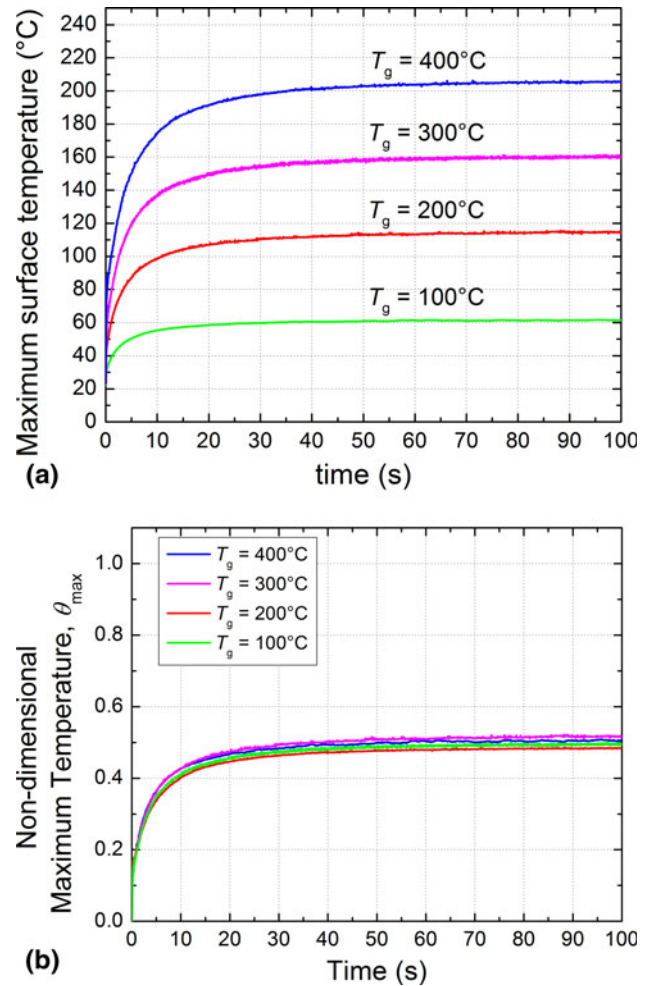
which would have induced variations in the surface temperature of the front of the substrate.

4.2 Effect of Substrate Thickness on the Surface Temperature Distribution

The thickness of the substrates will affect the surface temperature beneath the spreading compressed gas jet. Figure 5 shows the variation of the nondimensional surface temperature of steel 1020 as a function of the nondimensional radial distance from the stagnation point of the jet ($\xi = r/D$), where the radius (r) is normalized by the internal diameter of the cold spray exit nozzle (D). The figure shows that as the substrate thickness (z) increases, the maximum surface temperature at the stagnation point decreases. This is shown further in Fig. 6 in which the nondimensional thickness is $\Psi = (z/D)$. The substrates with lower thicknesses will have lower volumes through which to conduct heat. Therefore, the surface temperature remains high. As the distance from the stagnation point is increased beyond $\xi > 3$, the thicker substrate with $z = 6.2$ mm produced a surface temperature that was larger than that of the thinner substrate with
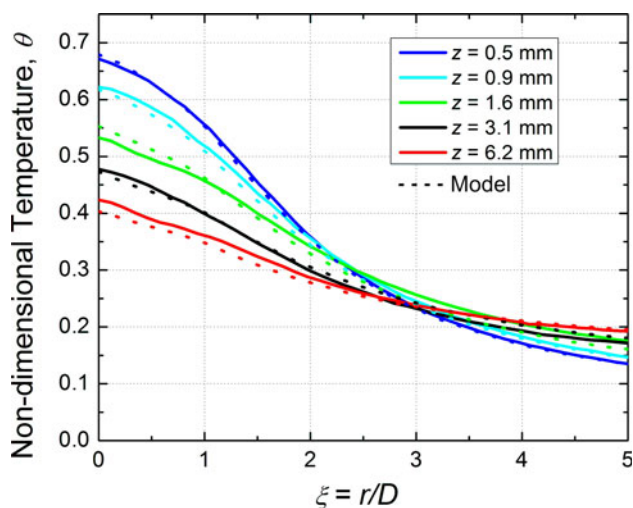
Fig. 5 Variation of the nondimensional surface temperature with the nondimensional radial distance from the jet stagnation point on steel 1020 substrates
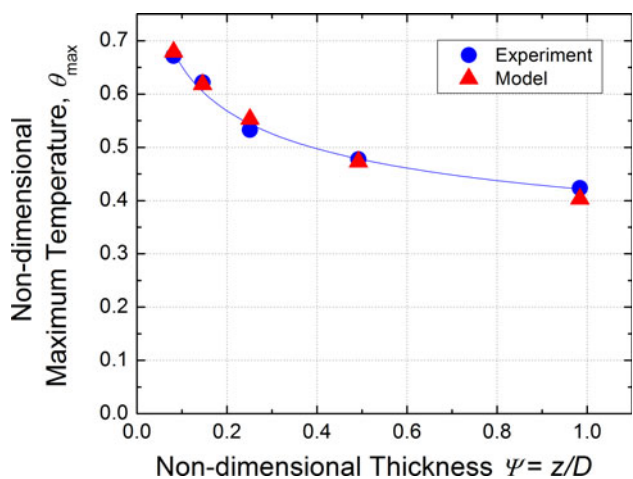

Fig. 6 Variation of the nondimensional maximum surface temperature with the nondimensional thickness of steel 1020 substrates

$z = 0.5$ mm. This was likely due to multidimensional conduction through the thick substrates, producing higher surface temperatures far from the stagnation point. The figures also present results from the computational model, which shows good agreement with the experimental results.

4.3 Effect of Substrate Properties on the Surface Temperature Distribution

The thermal properties of the substrate, in particular, the thermal conductivity, k_s, will affect the substrate surface temperature. Figure 7(a) and (b) shows that for substrates with a constant thickness of 1.6 mm, an increase in the thermal conductivity will produce a reduction in the surface temperature. As the thermal conductivity of the material increases, its ability to conduct heat increases to

produce lower surface temperatures. The combined effect of substrate thickness and thermal conductivity through use of the thermal conductance (kZ) for a wide range of materials (Lexan, stainless steel 304, steel 1020, aluminum 6061, pure aluminum, copper, and brass) is also presented in the figure (see Fig. 7c). As expected from Fig. 6, as the thermal conductance increases, the nondimensional maximum surface temperature decreases. The close agreement between the results of the numerical model and the experiments confirm that the model can be used to estimate the surface temperatures of a wide variety of substrate materials with different thicknesses.

### 4.4 Effect of Nozzle Motion on the Surface Temperature Distribution

Motion of the cold spray nozzle over the substrate surface will be required for fabrication of the coatings. It is expected that the effect of the moving nozzle and jet on the substrate temperature distribution and coating will differ from the case when the nozzle and jet are stationary. Figure 8(a) shows the surface temperature distribution of steel 1020 after single pass of the cold spray nozzle at velocities (V_t) between 2 and 150 mm/s. The gas jet temperature (as measured at the cold spray console) was 400 °C. The higher temperatures in the positive radial direction indicate that the nozzle completed its motion on that side of the substrate. The figure shows that the substrate surface temperature is higher when the nozzle traverses at lower speeds. The Peclét (Pe) number, which is a nondimensional measure of the ratio of convective diffusion due to the velocity of the moving jet to the conduction diffusion through the substrate, may be used to explain this observation. The Peclét number is defined as

$$\text{Pe} = \frac{V_t D}{\alpha_s} = \frac{\rho_s c_{ps} V_t D}{k_s}, \qquad \text{(Eq 8)}$$

where α_s, ρ_s, c_{ps}, and k_s are the substrate thermal diffusivity, density, specific heat capacity, and thermal conductivity, respectively.

For smaller values of the Peclét number, the temperature field penetrates significantly farther into the substrate from the impingement or stagnation point of the jet. Given that the material properties and nozzle diameter do not change significantly during impingement of the jet on the substrate surface, the nozzle velocity is the only variable that will induce direct changes in the Peclét number. Figure 8(b) shows that for smaller Peclét numbers, the nondimensional maximum temperature of the surface beneath the impinging jet is higher. This corresponds well with the results presented in and observations from Fig. 8(a).

Further observations of the influence of fluid velocity on the substrate temperature distribution can be seen in Fig. 9. The figure shows the effect of gas pressure (as measured at the cold spray console) and SOD on the radial surface temperature distribution of Lexan under a stationary jet. At a constant SOD of 10 mm, gas pressures of 690 kPa (100 psig) and 275 kPa (40 psig) produced approximately equal surface temperatures beneath the jet
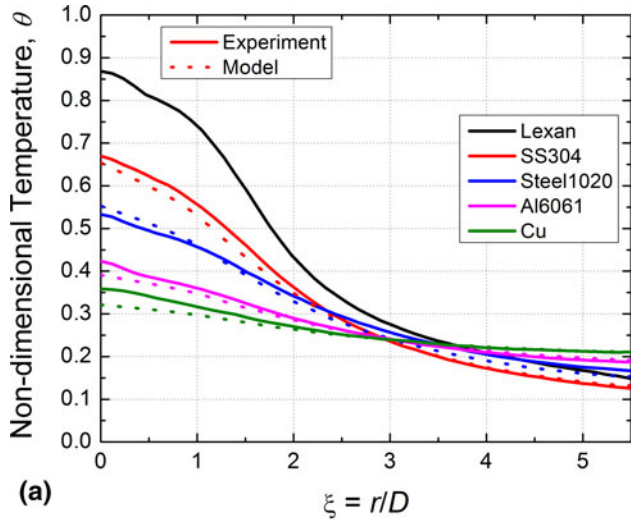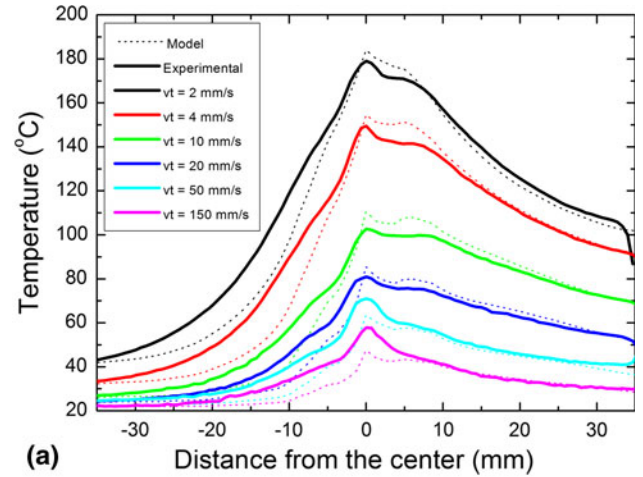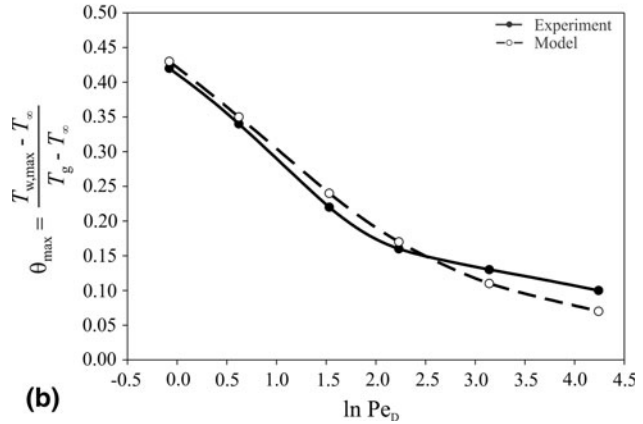
(a)
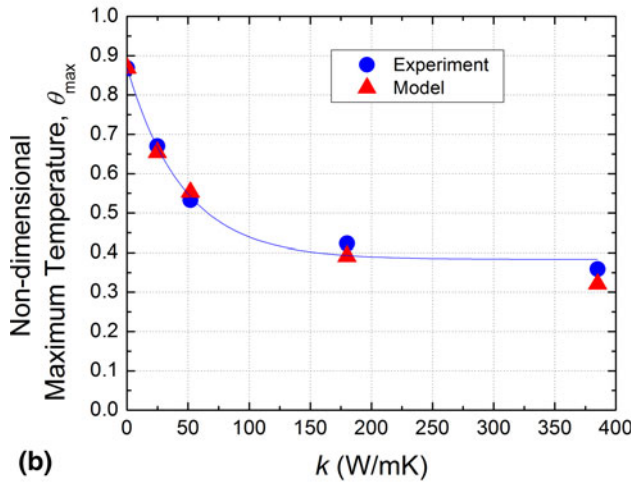
(b)
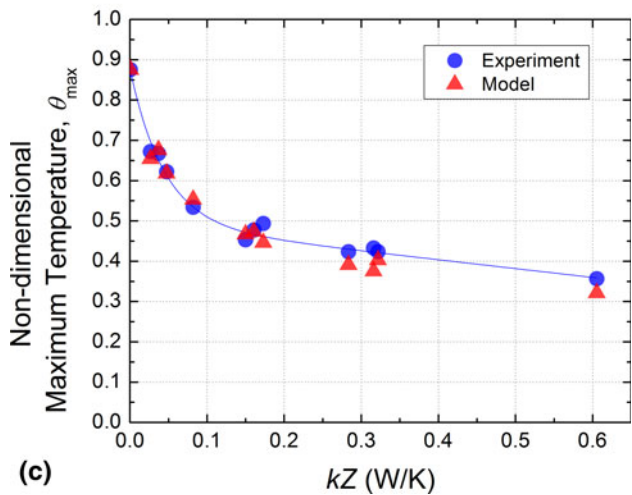
(c)

Fig. 7 Nondimensional temperature variation with (a) nondimensional radial distance from the jet stagnation point, (b) thermal conductivity, and (c) thermal conductance

at the stagnation point (see Fig. 9). It has been shown that the heat transfer coefficient at the stagnation point of the cold spray jet on the surface will be a maximum (Ref 21).

(a)

(b)

Fig. 8 Variation of the (a) surface temperature with the radial distance from the jet stagnation point (for different nozzle velocities) and (b) nondimensional maximum surface temperature with the natural logarithm of the Peclét number on steel 1020 substrates

It is well known that as the heat transfer coefficient increases to extremely large values, the surface temperature of the solid in contact with the moving fluid will be approximately the same as that of the fluid (Ref 22). Therefore, at low SOD, heat transfer will be enhanced and the nondimensional surface temperatures beneath the jet at the stagnation point are both nearly equal to 1, even though the gas pressures are different. As the SOD was increased to 40 mm at a gas pressure of 690 kPa (100 psig), the profile of the impinging jet on the surface changed, which changed the heat transfer coefficient. This increased SOD produced a reduction in the surface temperature beneath the stagnation point of the jet.

Away from the stagnation point, the substrate surface temperature was higher under the jet that was generated at 275 kPa (40 psig) than that generated by the jet at 690 kPa (100 psig), both at a SOD of 10 mm. The lower gas pressure produced a lower jet velocity during spreading along the substrate surface. This resulted in smaller values of the Peclét number, which induced greater thermal penetration through the substrate, away from the stagnation point of the jet.
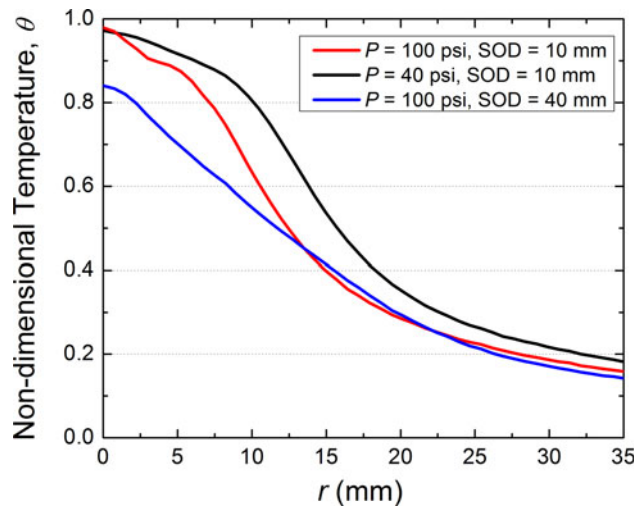
Fig. 9 Variation of the nondimensional surface temperature with the radial distance from the jet stagnation point on Lexan substrates for various gas pressures and SOD

5. Conclusions

The temperature distribution of the surfaces of several substrates under an impinging gas jet from a cold spray nozzle was determined and studied. The use of computer codes based on a finite differences method to solve a simplified 2D temperature distribution equation showed that a single profile of the transient nondimensional maximum surface temperature could be used to estimate the dimensional maximum surface temperature, regardless of the value of the compressed gas temperature. The close agreement of the numerical results with the experimental results suggested that the nondimensionalized results may be applied to a wide range of conditions and materials utilized in cold spraying.

This study has shown that the velocity of the nozzle and/or the jet will affect the temperature distribution of the substrate. It was found that the lower nozzle and/or jet velocities will produce increased substrate surface temperatures during cold spraying. The use of nondimensional temperatures and the nondimensional Peclét number will permit application of the results of this study to other values of velocity and gas temperatures that were not investigated in this present study.

While this study has presented some useful data and demonstrated the utility of a simple heat transfer model, further study still remains to be taken up. In particular, the intended study needs to be extended to the case where particles are included in the cold spray jet to fabricate a coating. At that point, it will be necessary to revaluate the heat transfer coefficient to determine the substrate surface temperature distribution.

References

1. A. Papyrin, V. Kosarev, K. Klinkov, A. Alkhimov, and V. Fomin, *Cold Spray Technology*, Elsevier, Oxford, UK, 2006
2. V. Champagne, *The Cold Spray Materials Deposition Process: Fundamentals and Applications*, Woodhead Publishing Limited, Cambridge, UK, 2007
3. R. Maev and V. Leshchinsky, *Introduction to Low Pressure Gas Dynamic Spray: Physics and Technology*, Wiley-VCH Verlag GmbH, Weinheim, 2008
4. E. Irissou, J.G. Legoux, A. Ryabinin, B. Jodoin, and C. Moreau, Review on Cold Spray Process and Technology: Part I—Intellectual Property, *J. Therm. Spray Technol.*, 2008, **17**, p 495-516
5. P. King, G. Bae, H. Zahiri, M. Jahedi, and C. Lee, An Experimental and Finite Element Study of Cold Spray Copper Impact onto Two Aluminum Substrates, *J. Therm. Spray Technol.*, 2010, **19**, p 620-634
6. H. Assadi, F. Gartner, T. Stoltenhoff, and H. Kreye, Bonding Mechanism in Cold Gas Spraying, *Acta Mater.*, 2003, **51**, p 4379-4394
7. M. Grujicic, C. Zhao, W. De-Rosset, and D. Helfritch, Adiabatic Shear Instability Based Mechanism for Particles/Substrate Bonding in the Cold-Gas Dynamic-Spray Process, *Mater. Des.*, 2004, **25**, p 681-688
8. T. Schmidt, F. Gartner, H. Assadi, and H. Kreye, Development of a Generalized Parameter Window for Cold Spray Deposition, *Acta Mater.*, 2006, **54**, p 729-742
9. T. Schmidt, H. Assadi, F. Gärtner, H. Richter, T. Stoltenhoff, H. Kreye, and T. Klassen, From Particle Acceleration to Impact and Bonding in Cold Spraying, *J. Therm. Spray Technol.*, 2009, **18**, p 794-808
10. M. Fukumoto, H. Wada, K. Tanabe, M. Yamada, E. Yamaguchi, A. Niwa, M. Sugimoto, and M. Izawa, Effect of Substrate Temperature on Deposition Behavior of Copper Particles on Substrate Surfaces in the Cold Spray Process, *J. Therm. Spray Technol.*, 2007, **16**, p 643-650
11. W. Wong, E. Irissou, A. Ryabinin, J.G. Legoux, and S. Yue, Influence of Helium and Nitrogen Gases on the Properties of Cold Gas Dynamic Sprayed Pure Titanium Coatings, *J. Therm. Spray Technol.*, 2010, **20**, p 213-226
12. J.G. Legoux, E. Irissou, and C. Moreau, Effect of Substrate Temperature on the Formation Mechanism of Cold-Sprayed Aluminum, Zinc, and Tin Coatings, *J. Therm. Spray Technol.*, 2007, **16**, p 619-626
13. D. Goldbaum, J.M. Shockley, R. Chromik, A. Rezaeian, S. Yue, J.G. Legoux, and E. Irissou, The Effect of Deposition Conditions on Adhesion Strength of Ti and Ti6Al4V Cold Spray Splats, *J. Therm. Spray Technol.*, 2012, **21**, p 288-303
14. M. Kulmala and P. Vuoristo, Influence of Process Conditions in Laser-Assisted Low-Pressure Cold Spraying, *Surf. Coat. Technol.*, 2008, **202**, p 4503-4508
15. Y. Danlos, S. Costil, X. Guo, H. Liao, and C. Coddet, Ablation Laser and Heating Laser Combined to Cold Spraying, *Surf. Coat. Technol.*, 2010, **205**, p 1055-1059
16. R. Lupoi, M. Sparkes, A. Cockburn, and W. O'Neill, High Speed Titanium Coatings by Supersonic Laser Deposition, *Mater. Lett.*, 2011, **65**, p 3205-3207
17. S. Rech, A. Trentin, S. Vezzù, J.G. Legoux, E. Irissou, and M. Guagliano, Influence of Pre-heated Al 6061 Substrate Temperature on the Residual Stresses of Multipass Al Coatings Deposited by Cold Spray, *J. Therm. Spray Technol.*, 2010, **20**, p 243-251
18. P. King, S. Zahiri, and M. Jahedi, Microstructural Refinement Within a Cold-Sprayed Copper Particle, *Metall. Mater. Trans. A*, 2009, **40A**, p 2115-2123
19. V. Kosarev, S. Klinkov, A. Alkhimov, and A. Papyrin, On Some Aspects of Gas Dynamics of the Cold Spray Process, *J. Therm. Spray Technol.*, 2003, **12**, p 265-281
20. W. Li, S. Yin, X. Guo, H. Liao, X. Wang, and C. Coddet, An Investigation on Temperature Distribution Within the Substrate and Nozzle Wall in Cold Spraying by Numerical and Experimental Methods, *J. Therm. Spray Technol.*, 2012, **21**, p 41-48
21. A. Ryabinin, E. Irissou, A. McDonald, and J.G. Legoux, Simulation of Gas-Substrate Heat Exchange During Cold Gas Dynamic Spraying, *Int. J. Thermal Sci.*, 2012, **56**, p 12-18
22. D. Poulikakos, *Conduction Heat Transfer*, Prentice Hall, Englewood Cliffs, NJ, 1994